MJFAS
Malaysian Journal of Fundamental and Applied Sciences

Sahapini *et al.* | Malaysian Journal of Fundamental and Applied Sciences, Vol. 21 (2025) 2825–2843

RESEARCH ARTICLE

The Role of Mixed Alkaline Earth Effects on The Elastic Properties of $xBaF_2$–$(50 – x)CaF_2$–$50B_2O_3$ Fluoroborate Glasses: Comparative Analysis of Ultrasonic Measurements and Theoretical Models

N. F. M. Sahapini[a], R. Hisam[b]*, M. Mazlan[a], R. A. A. Wahab[a], M. Mohammad[a]

[a]Faculty of Applied Sciences, Universiti Teknologi MARA, Perak Branch, Tapah Campus, 35400 Tapah Road, Perak, Malaysia; [b]Faculty of Applied Sciences, Universiti Teknologi MARA, 40450 Shah Alam, Selangor, Malaysia

Abstract The incorporation of fluoride ions (F^-) as glass modifiers in oxide glasses has garnered considerable interest due to their benefits in various advanced applications (solar energy conversion, laser systems, infrared fiber optics, electronic devices). A deeper understanding of the elastic properties of fluoroborate glasses is crucial for exploring the unique structural features they exhibit. In particular, studying the mixed alkaline earth effect (MAEE) is important, as it introduces compositional variations that alter both structure and mechanics of the glass network. This study focuses on the elastic behavior of $xBaF_2$–$(50 – x)CaF_2$–$50B_2O_3$ glasses (x = 5–35 mol%), synthesized via melt-quenching. Ultrasonic velocity measurements were used to probe the elastic moduli, providing key insights into material stability and performance. Three theoretical models (Makishima–Mackenzie, Bulk Compression, Ring Deformation) were employed to interpret the results. The elastic moduli, particularly longitudinal and bulk moduli, exhibit non-linear compositional trends with two distinct minima at 10 and 25 mol% BaF_2. These deviations from linearity are attributed to MAEE-induced phase separation and disrupted cross-linking in the glass network. Such non-linearity reveals underlying structural heterogeneity; for example, certain mixed-cation compositions likely promote local phase separation or network fragmentation, which in turn softens the glass. Notably, the Makishima–Mackenzie model shows a drop in overall bond dissociation energy at 25 mol% BaF_2, indicating a significant structural change at this composition. Meanwhile, the Bulk Compression model suggests that elasticity is governed by bond-length adjustments (without bond-angle changes), and the Ring Deformation model points to isotropic borate ring compression as the dominant elastic mechanism. Understanding these MAEE, driven anomalies is practically advantageous for materials engineers to pinpoint compositions that either maximize rigidity or, conversely, signal structural weaknesses. Our findings demonstrate that MAEE can be harnessed to tailor the elastic behaviour and mechanical stability of fluoroborate glasses, enhancing their potential for high-performance applications requiring robust and reliable glass materials.

Keywords: Mixed alkaline earth effects (MAEE), Elastic properties, Bulk compression model, Makishima-Mackenzie theory, Alkaline earth fluoride, Mixed modifier effects (MME).

***For correspondence:**
rosdiyana@uitm.edu.my

Received: 26 Sept. 2024
Accepted: 2 Sept. 2025

Introduction

Glasses are non-crystalline materials or amorphous solids because they lack the long-range order of an atomic structure [1]. The variety of uses and applications of glass depends on its properties, which are

determined by the composition and modifying components in the glass former [2, 3]. Borate (B_2O_3) is one of the best oxide glass formers because it exhibits high glass forming ability, low melting temperature, high thermal stability, and high chemical resistance [4]. The compound also possesses a small cation size and high atomic bond strength, which enhances its durability and stability [5]. Additionally, the coordination number of borate can change from three to four when alkali or alkaline earth cations are introduced, resulting in unique properties related to the change in structure and elasticity of the resulting glasses [5], [6].

The incorporation of borate-containing fluoride ions as glass modifiers has garnered attention due to its benefits in various applications, such as solar energy converters, lasers, infrared fibre optics, and electronic devices. Moreover, fluoride-containing glasses exhibits relatively high moisture resistant [7] and demonstrate greater mechanical strength [8], [9] compared to other alkali borate glasses. Consequently, structural studies of binary fluoroborate CaF_2–B_2O_3 and BaF_2–B_2O_3 glasses have been performed to investigate the role of fluoride ions (F^-) [10]. This investigation revealed a large glass-forming region in the oxyfluoride systems, which was excellent and easy to form. Additionally, it was found that most fluorides entered the glass network and converted the BO_3 units into BO_3F (B_4 units) with B–F linkages. Other studies on NaO–NaF–B_2O_3 [11] also demonstrated that monovalent F^- ions formed non-bridging B–F bonds and partially disconnected the six-membered rings with $BO_{4-z}F_z$ tetrahedra from the rest of the borate network.

Mixed alkali effects (MAE) represent the non-linear relations of physical properties associated with alkali ions' movement and structural properties when a type of alkali ion in a glass is gradually replaced by a different kind of ion at a constant total alkali oxide concentration. Research on MAE revealed that numerous physical properties, notably ionic conductivity, activation energy, glass transition temperature, and viscosity, exhibited remarkable deviation from the linearity [12], [13]. Similar effects were observed in mixed alkaline-earth glasses (MAEE) [14], where significant deviations from linearity were reported in density, packing fraction, activation energy, and all mechanical properties.

Previous investigations on the structure of MAEE (40 − *x*)SrO−*x*BaO−45SiO_2−10B_2O_3− 5ZrO_2 (*x* = 0, 10, 20, 30, and 40 mol%) glass system [15] have demonstrated that the deviation of linearity in the molar volume (V_m) with the change of BaO concentration in glass was associated with the presence of two alkaline modifiers. Additionally, the modifiers have been reported to induce micro-heterogeneities or local segregation that disturb the cross-linking in the glass matrix due to varying field strength, electronegativity, and local chemical environment among the glass constituents [15]. In our system, XRD measurements confirm that all compositions remain amorphous, excluding long-range crystallisation. However, anomalies observed in density, molar volume, and elastic moduli, together with earlier optical and spectroscopic data on the same glasses [16], suggest that the non-linear trends are consistent with MAEE-driven structural disorder within the amorphous network. Direct microstructural characterisation (e.g., FESEM or TEM) would be valuable to confirm such nanoscale features and remains a direction for future work.

Besides that, these structural anomalies can be explained by the presence of non-bridging oxygen (NBO) and non-bridging fluorine (NBF) atoms. NBOs are generated when boron atoms form fewer bridging linkages than in a fully connected BO_4 tetrahedral network, which weakens the connectivity and reduces stiffness [11], [17]. Similarly, fluorine substitution for bridging oxygen creates NBFs, resulting in B–F bonds that depolymerise the glass network [11], [18]. Because B–F bonds are weaker and less directional compared to B–O bonds, their presence increases free volume and lowers resistance to compression and shear [6], [9]. Both NBO and NBF units are therefore key contributors to the observed non-linear elastic behaviour, as they directly disrupt cross-linking density and modify the rigidity of the glass matrix. Their formation is especially relevant in mixed alkaline earth systems, where variations in cation field strength and ionic radius intensify these effects.

Generally, structural changes in glasses are closely related to elastic properties. The ultrasonic velocity measurement technique, which is sensitive to glass network changes and compactness, is useful in studying the elastic properties of glasses [19], [20]. Previous ultrasonic studies of several fluoroborate glass systems, such as (70 – *x*)B_2O_3–30BaF_2–*x*LiF [21], 20Na_2O–(20 – *x*)ZnO– *x*ZnF_2–60B_2O_3 [22], and 60B_2O_3–(40 − *x*)PbO–*x*PbF_2 [23], have provided insights into how the compositions and addition of fluoride modifiers contributed to changes in the rigidity and elastic moduli of glasses. Ultrasonic studies on BaF_2–TeO_2 glasses have revealed that the ultrasonic attenuation coefficient increases with higher BaF2 content, leading to a decrease in density, ultrasonic velocities, and glass transition temperature [18]. Additionally, research on *x*MgO–(50 – *x*)CaO–50SiO_2, showed a clear indication of the MAEE in the elastic moduli (K, L, S, and Y), suggesting affecting ion conduction. The specific role of F- in modifying ultrasonic velocities and elastic moduli in MAEE may contribute to the significant knowledge gaps as

they could support a comprehensive understanding of the structural and optical properties. Besides, understanding elastic properties of fluoroborate MAEE is essential, as it also rely on the structure of glass and ion conduction. In addition, it is also crucial to initiate research on elastic behaviour in mixed alkaline fluoroborate glass that employs multiple theoretical models to understand how the mixed alkaline earth effect behaves and gain insights into the function of F- in the glass system. Conducting elastic studies with the aid of ultrasonic measurements would offer more detailed insights into the stiffness, rigidity, cross-linking, and ring deformation in the transition areas influenced by a mixed alkaline earth environment.

Therefore, in this current study, the ultrasonic velocity of xBaF$_2$–(50 – x)CaF$_2$–50B$_2$O$_3$ glasses was measured to investigate the influence of MAEE on elastic properties. Furthermore, the study determined experimental values for longitudinal (L), shear (S), bulk (K_e), and Young's (Y) moduli, Poisson's ratio (σ), microhardness (H), and Debye temperature (θ_D). The theoretical approach based on the Makishima-Mackenzie and bond compression models was also discussed.

Materials and Methods

Ternary fluoroborate glass samples of xBaF$_2$–(50 – x)CaF$_2$–50B$_2$O$_3$ (x = 5 to 35 mol%) were prepared using the conventional melt-quenching method. High-purity analytical grade BaF$_2$ (99.99% purity), CaF$_2$ (99.99% purity), and B$_2$O$_3$ (99.999% purity) commercial powders were accurately weighed and thoroughly mixed. The powder mixture was then continuously ground using an agate mortar and pestle for one hour to ensure a fine and homogeneous blend. Subsequently, the mixed powder was placed in an alumina crucible, covered, and melted in a furnace at 1000 °C for one hour.

After the melting process, the molten glass was rapidly poured into a pre-heated stainless-steel mold maintained at 350 °C for three hours. This step was essential to minimize the mechanical stresses that can occur during the quenching process. Subsequently, the glass sample was allowed to cool to room temperature.

The density (ρ) of the glass samples was measured according to Archimedes' Principle. The weight of the glass in air and liquid (immersed in toluene) was determined. Subsequently, the density was calculated according to equation (1), while the molar volume was determined with equation (2).

$$\text{Density, } \rho = \frac{W_{air}}{W_{air} - W_l}\rho_l \quad (1)$$

$$\text{Molar volume, } V_m = \frac{M}{\rho} \quad (2)$$

W_{air} is the weight of the sample in air, W_l is the weight in the immersion liquid, ρ_l is the density of the immersion liquid, toluene, 0.8690 g cm^{-3} at 25 °C, and M is the molecular weight of the glass sample. Before ultrasonic measurements, the bulk samples were polished with fine sandpapers approximately 4 to 5 mm thickness to obtain smooth parallel surfaces on both sides. The ultrasonic wave velocities (longitudinal and shear) were recorded at room temperature at 5 MHz via the pulse-echo technique with a RITEC RAM-500-M6 high-performance ultrasonic. The longitudinal and shear velocities were determined based on the relation $v = 2d/t$ [24], where d is the thickness of the samples and t is the round-trip delay time obtained from the oscilloscope pulse. The elastic constants, L, S, Y, K_e, θ_D, H, σ, and v_m, were determined with equations (3) to (10) [25], [26].

$$\text{Longitudinal modulus, } L = \rho {v_L}^2 \quad (3)$$

$$\text{Shear modulus, } S = \rho {v_S}^2 \quad (4)$$

$$\text{Young's modulus, } Y = \frac{9K_eS}{3K_e + S} \quad (5)$$

$$\text{Bulk modulus, } K_e = L - \frac{3}{4}S \quad (6)$$

Debye temperature, $\theta_D = \left(\frac{h}{k_b}\right)\left(\frac{3PN_a}{4\pi V_m}\right)^{\frac{1}{3}} v_m$ (7)

Hardness, $H = \frac{(1-2\sigma)Y}{6(1+\sigma)}$ (8)

Poisson's ratio, $\sigma = \frac{L-2S}{2(L-S)}$ (9)

Mean velocity, $v_m = \left[\frac{3v_L^3 v_S^3}{v_L^3+2v_S^3}\right]^{\frac{1}{3}}$ (10)

Where v_L and v_S are longitudinal and shear velocities, respectively, h is Planck's constant, k_b is Boltzmann's constant, N_a is Avogadro's number, P is the number of atoms in the chemical formula, and V_m is the molar volume.

Results and Analysis

Density and Molar Volume

The variations in ρ and V_m of the xBaF$_2$–(50 – x)CaF$_2$–50B$_2$O$_3$ (x = 5 – 35 mol%) glass samples are listed in Table 1. As shown in Figure 1, increasing the BaF$_2$ content in the samples led to an increase in ρ from 2822 to 3252 kg m^{-3} (error bar for density cannot be shown due to very small standard deviation compared to actual value) and an increase in V_m from 2.79 × 10^{-5} to 3.32 × 10^{-5} m^3 mol^{-1}. Although glasses typically exhibit a decrease in V_m as ρ increases [27], [28], the opposite behaviour was observed in the present study. These findings are consistent with similar observations in studies on MAEE glasses, such as xMgO–(50 – x)CaO–SiO$_2$ glass [14] and xMgO–(30 – x)BaO–69.8B$_2$O$_3$–0.2Cr$_2$O$_3$ [29]. Additionally, an off-trend observation occurred at x = 25 mol% BaF$_2$, where there was a dramatic increase ρ, while V_m demonstrated a sudden drop.

Table 1. The ρ and V_m of the xBaF$_2$−(50 − x)CaF$_2$−50B$_2$O$_3$ (x = 5 to 35 mol%) glass samples

x (mol%)	ρ (kg m^{-3})	V_m (× 10^{-5} m^3 mol^{-1})
5	2821.53 ± 0.89	2.79
10	2918.45 ± 0.52	2.86
15	2985.74 ± 0.39	2.96
20	3065.01 ± 0.35	3.04
25	3320.23 ± 0.44	2.96
30	3185.99 ± 1.42	3.23
35	3252.34 ± 0.37	3.32

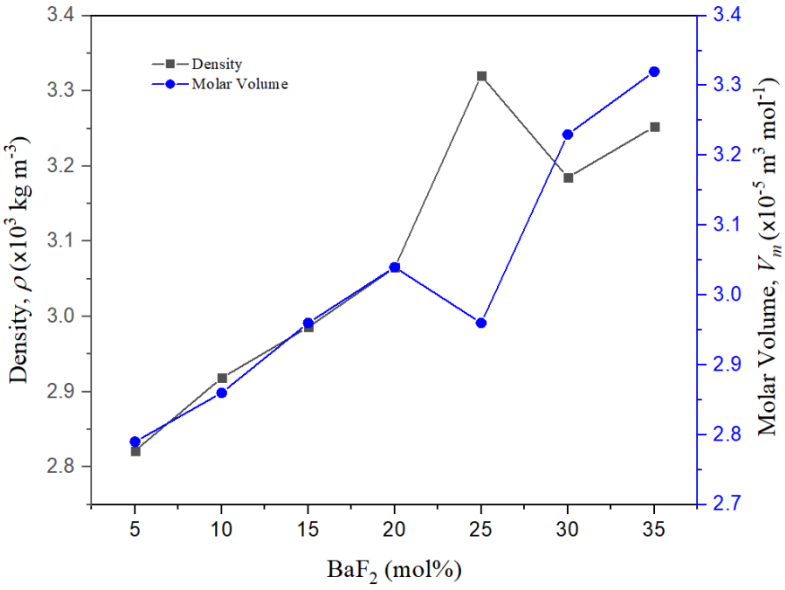

Figure 1. The ρ and V_m of the xBaF$_2$−(50 − x)CaF$_2$−50B$_2$O$_3$ (x = 5 – 35 mol%) glass samples

Experimental Elastic Properties

Figure 2 shows the plot of longitudinal velocity (v_L) and shear velocity (v_S) data against the change of BaF$_2$ content, indicating a general reduction in both values as the BaF$_2$ content increases. Upon closer inspection, v_L exhibited a sharp decline at 10 and 25 mol% but increased again up to 35 mol%. On the other hand, v_S decreased between 5 to 30 mol%, with a drastic reduction observed at 20 mol% before escalating abruptly at 35 mol%. Interestingly, the v_L and v_S trends observed in this study differed from previous investigations on glasses with different compositions, which showed almost identical v_L and v_S patterns [25], [27], [30].In addition to these velocity values, Table 2 provides the corresponding calculated values for longitudinal modulus (L), shear modulus (S), Young's modulus (Y), bulk modulus (K_e), Debye Temperature (θ_D), Poisson's ratio (σ) and Hardness (H). Graphs illustrating the changes in L, S, K_e, and Y with varying BaF$_2$ content are presented in Figure 3 and Figure 4.

The L and K_e values variations closely followed v_L, with two minima observed at 10 and 25 mol% of BaF$_2$. On the other hand, S and Y exhibited a similar trend to v_S, with a drastic drop at x = 20 mol% followed by an increase again at 35 mol%. Figure 5 summarizes the changes in θ_D and v_m values of the glass system under study. Throughout the addition of BaF$_2$, both θ_D and v_m decreased, with a slightly more significant drop at 20 mol%, before quickly escalating at 35 mol%. Meanwhile, the σ exhibited nonlinear fluctuations similar to L and K_e, while H showed an opposite trend to σ. The values for σ ranged from 0.24 to 0.30.

Table 2. The Values of v_L, v_S, v_m, L, S, Y, K_e, θ_D, σ, and H of xBaF$_2$−(50 − x)CaF$_2$−50B$_2$O$_3$ (x = 5 − 35 mol%) Glass System

x (mol%)	v_L ± 0.01 (km s^{-1})	v_S ± 0.01 (km s^{-1})	v_m ± 0.02 (km s^{-1})	L ± 0.37 (GPa)	S ± 0.20 (GPa)	Y ± 2.00 (GPa)	K_e ± 0.60 (GPa)	θ_D ± 0.50 (K)	σ ± 0.01	H ± 0.30 (GPa)
5	6.323	3.444	3.841	112.82	33.46	86.27	68.20	441	0.29	4.70
10	5.804	3.397	3.766	98.30	33.68	83.49	53.39	436	0.24	5.85
15	5.910	3.270	3.643	104.27	31.93	81.69	61.71	425	0.28	4.70
20	5.705	3.024	3.379	99.74	28.03	73.13	62.37	397	0.30	3.65
25	5.168	2.922	3.249	88.66	28.34	71.71	50.88	391	0.27	4.44
30	5.331	2.861	3.194	90.51	26.07	67.66	55.75	379	0.30	3.52
35	5.474	3.049	3.394	97.44	30.23	57.13	77.10	405	0.28	4.53

e-ISSN 2289-599X| DOI: https://doi.org/10.11113/mjfas.v21n6.3892

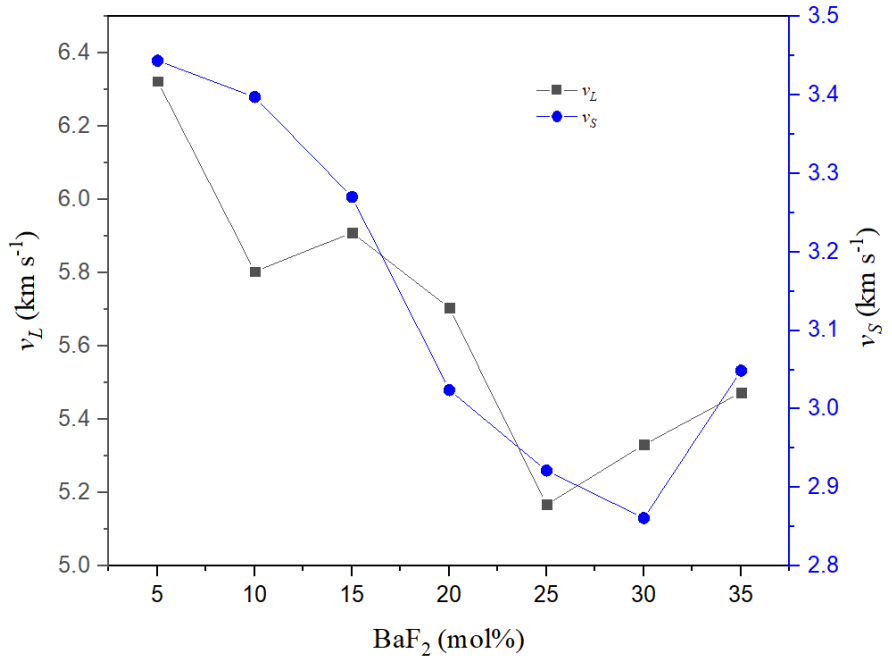

Figure 2. The plotted v_L and v_S values of the xBaF$_2$–(50 – x)CaF$_2$ –50B$_2$O$_3$ (x = 5 to 35 mol%) glass samples

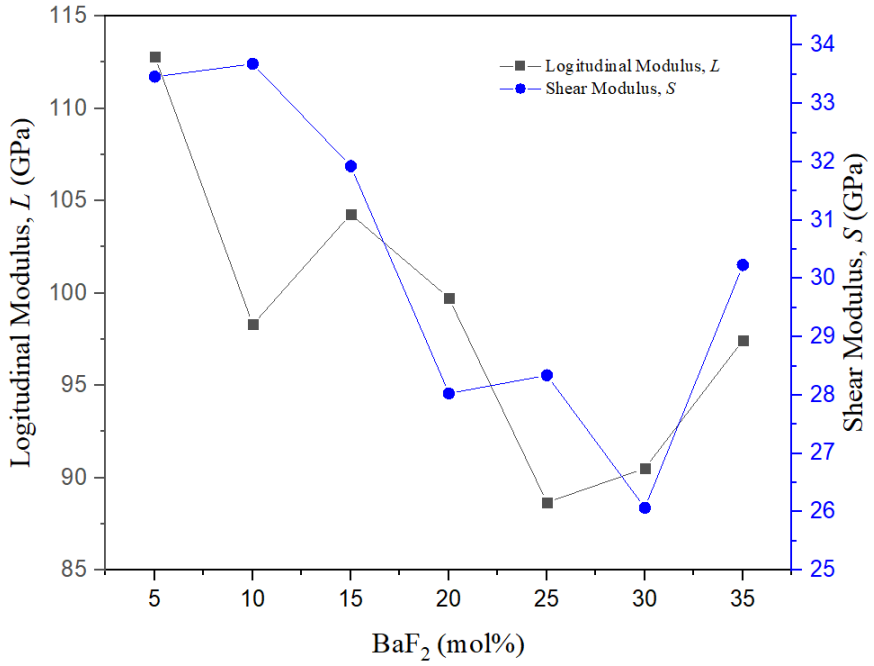

Figure 3. The plotted L and S values of the xBaF$_2$–(50 – x)CaF$_2$–50B$_2$O$_3$ (x = 5 to 35 mol%) glass samples

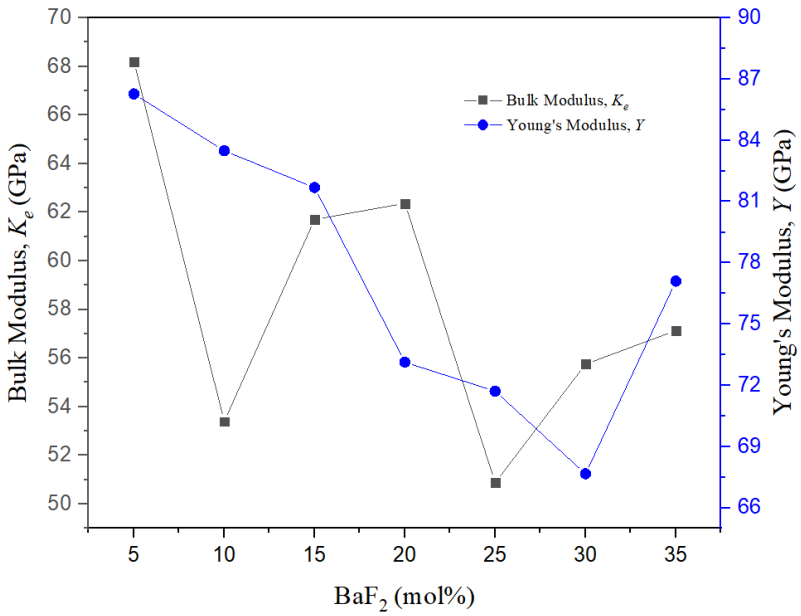

Figure 4. The plotted K_e and Y values of the xBaF$_2$–(50 – x)CaF$_2$–50B$_2$O$_3$ (x = 5 to 35 mol%) glass samples

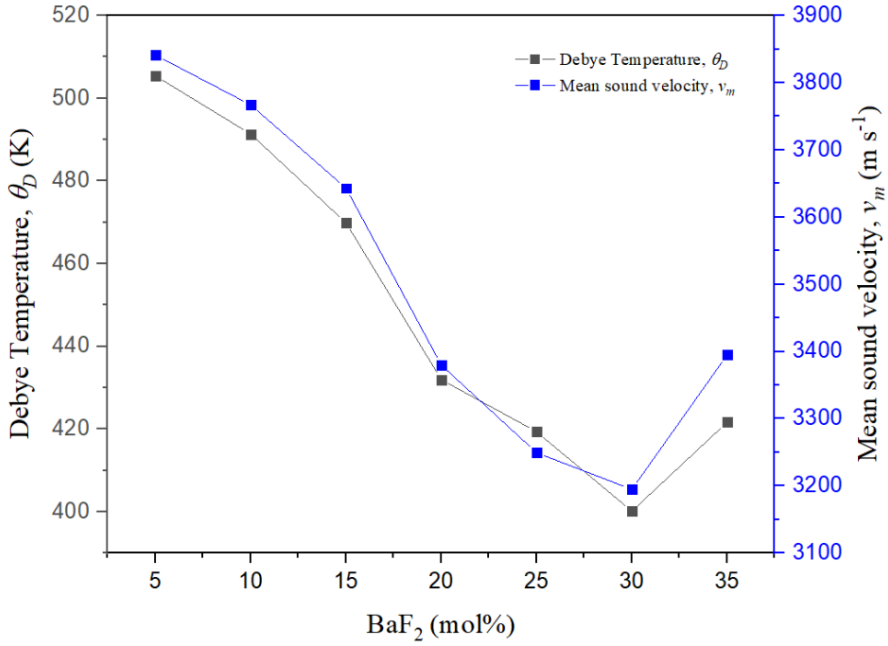

Figure 5. The plotted θ_D and v_m values of the xBaF$_2$–(50 – x)CaF$_2$–50B$_2$O$_3$ (x = 5 to 35 mol%) glass samples

Theoretical Elastic Model

Quantitative analysis of experimental elastic moduli can be performed using three theoretical models: the Makishima-Mackenzie model [31], the bond compression model, and the ring deformation model [32]. The Makishima-Mackenzie model calculates theoretical elastic moduli values based on packing density and dissociation energy values, considering the atomic arrangement in the material and the energy required to dissociate the bonds between atoms. The bond compression model, on the other

hand, considers the atomic geometry of oxides, including bond length and coordination number [33], to determine elastic moduli by considering the distances between atoms and their coordination with neighbouring atoms. The ring deformation model involves observing changes in ring size (*l*) through the ratio of K_{bc}/K_e, focusing on changes in the size of rings formed by atoms in the material and their effects on the elastic properties.

The Makishima-Mackenzie Model

Theoretical Y values from the Makishima-Makenzie model were calculated using equation (11) [31], [34], [35], after determining the dissociation energy with equation (12). The packing density of the compound A_aO_b was found by employing equation (13) [23], while the packing factor was calculated with equation (14)[36].

$$\text{The Makishima-Makenzie Young's modulus, } Y_{M-M} = 8.36\, V_t G_t \tag{11}$$

$$\text{Dissociation energy, } G_t = \sum_i G_i\, x_i \tag{12}$$

$$\text{Packing density, } V_t = \frac{1}{V_m}\sum_i V_i\, x_i \tag{13}$$

$$\text{Packing factor, } V_i = 4\pi N_a (aR_A^3 + bR_O^3)/3 \tag{14}$$

Where G_t represents the dissociation energy per unit volume of glass, G_i is the dissociation energy per unit volume of the oxide or fluoride component (*i*), x_i is the mole fraction of the component, V_i is the atomic volume or packing factor of the component (*i*), V_m is the molar volume of the glass, N_a is Avogadro's number, and R_A and R_O are Pauling's ionic radii of the cation and oxide or fluoride, respectively. Dissociation energies per unit volume, (G_i) of B_2O_3, BaF_2, and CaF_2 for the glass system xBaF$_2$–(50 – x)CaF$_2$–50B$_2$O$_3$ (x = 5 to 35 mol%) were obtained directly from [37] and presented in Table 3.

Table 3. The reference values of ρ, molar mass (M), bond length (r), stretching force (f), coordination number (n_f), cross-link density per cation (n_c), V_i, and G_i of the BaF_2, CaF_2, and B_2O_3 components

Oxide or fluoride	ρ (× 10^3 kg m^{-3})	M (g mol^{-1})	r (nm)	f (N)	n_f	n_c	V_i (× 10^6 m^3 mol^{-1})	G_i (×10^6 kJ m^{-3})	Ref
BaF_2	4.89	175.34	0.230	212.50	10	8	18.57	89.6	[37], [38], [39], [40]
CaF_2	3.18	78.07	0.200	139.72	8	6	14.39	132.2	[37]
B_2O_3	2.55	69.63	0.137	661.13	3	1	20.79	15.6	[17]
			0.148	524.40	4	2		82.8	

In the current study, borate glass was used as the former glass. The coordination number of borate has been reported to change from three to four with alkali or alkaline earth contents [41], [42]. Previous studies have also demonstrated that coordination numbers affect the elastic properties of the glass systems. Therefore, when calculating the dissociation energy per unit volume of B_2O_3 using equation (15), the change of coordination number must be considered [17].

From equation (15), N_4 represents the ratio of 4 coordinated boron units to all boron units which the data were sourced from previous reports on the structural and optical properties of the studied glasses [16]. Additionally, G_4 and G_3 denote the dissociation-free energies of the pure four and three-coordinate components respectively.

Table 4 summarizes the theoretical Young's modulus ($Y_{M\text{-}M}$), bulk modulus ($K_{M\text{-}M}$), shear modulus ($S_{M\text{-}M}$), longitudinal modulus ($L_{M\text{-}M}$) and Poisson's ratio ($\sigma_{M\text{-}M}$) based on the Makishima-Mackenzie model, all calculated in GPa, with the G_t in kcal/cm^3. These theoretical elastic moduli of a multi-component oxide glass, expressed in V_t and G_t, were calculated using equations (16) to (19) [20] and were observed higher than the experimental values. However, these calculated values decrease, with a drop at 25 mol% as shown in Figure 6. Similarly, $\sigma_{M\text{-}M}$ values decrease slightly, ranging from 0.28 and 0.26.

$$G_B = N_4 G_4 + (1 - N_4) G_3 \quad (15)$$

$$\text{Bulk modulus, } \mathrm{K_{M-M}} = 10.0\ \mathrm{V_t^2 G_t} \quad (16)$$

$$\text{Shear modulus, } \mathrm{S_{M-M}} = {30.0\ \mathrm{V_t^2 G_t}}/{(10.2\ \mathrm{V_t} - 1)} \quad (17)$$

$$\text{Longitudinal modulus, } \mathrm{L_{M-M}} = \mathrm{K_{M-M}} + 4\mathrm{S_{M-M}}/3 \quad (18)$$

$$\text{Poisson's ratio, } \mu_{\mathrm{M-M}} = 0.5 - (1/7.2\ \mathrm{V_t}) \quad (19)$$

Table 4. The elastic moduli, N_4, V_t, and G_t values calculated according to the Makishima-Mackenzie model of the xBaF$_2$–(50 – x)CaF$_2$–50B$_2$O$_3$ (x = 5 to 35 mol%) glass system

x (mol%)	$Y_{M\text{-}M}$ (GPa)	$K_{M\text{-}M}$ (GPa)	$S_{M\text{-}M}$ (GPa)	$L_{M\text{-}M}$ (GPa)	$\sigma_{(M\text{-}M)}$ (GPa)	N_4	V_t	G_t (kcal/cm^3)
5	119.73	91.37	49.81	157.78	0.28	0.659	0.638	22.45
10	113.95	86.12	47.84	149.91	0.28	0.632	0.630	21.72
15	110.67	81.81	46.73	144.12	0.27	0.680	0.615	21.60
20	105.77	77.15	44.99	137.14	0.27	0.669	0.606	21.00
25	91.38	67.32	37.47	117.28	0.28	0.290	0.621	17.45
30	98.82	69.57	42.60	126.37	0.26	0.726	0.583	20.44
35	93.43	64.63	40.32	118.39	0.26	0.688	0.574	19.63

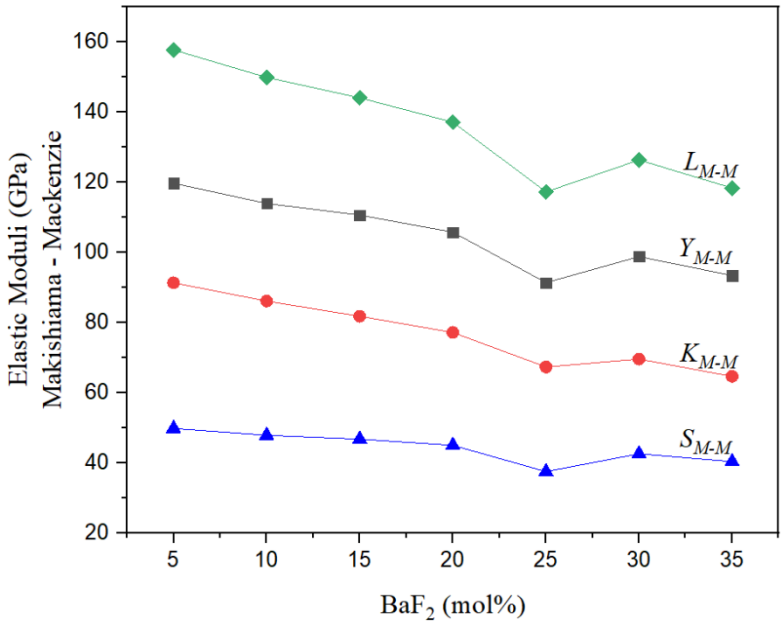

Figure 6. The theoretical Makishima-Mackenzie elastic moduli values (Y_{M-M}, K_{M-M}, S_{M-M}, and L_{M-M}) against the change in BaF_2 content

The Bulk Compression Model

A previous investigation reported findings on theoretical elastic moduli known as the bulk compression model, K_{bc}, as the continuation of the Makishima-Mackenzie study [32]. The K_{bc} can be determined using equation (20) [28] for three-dimensional network structures. The first-order stretching force constant for each oxide, f_i, was determined by equation (21) [28].

$$\text{Bond compression bulk modulus, } K_{bc} = \frac{N_a}{9V_m}\sum_i x_i\, n_f f_i r_i^2 \quad (20)$$

$$\text{First-order stretching force, } f_i = \frac{1.7}{r_i^3} \quad (21)$$

For equation (20) and equation (21), x_i represents the mole fraction of the oxide/fluoride component, n_f is the coordination number of the cations, N_a is Avogadro's number, r_i is the bond length, and i denotes the oxide/fluoride component. To determine the average coordination number of B_2O_3 components, equation (22) was utilized [28], [43]. This equation facilitated the establishment of the average B-O-B bond length (r_{B2O3}) in the presence of both three and four-coordinated boron atoms within the glass network [44].

$$n_{f\ ave} = (4-3)xN_4 + 3 \quad (22)$$

$$r_{B_2O_3} = \left(r_{BO_4} - r_{BO_3}\right) xN_4 + r_{BO_3} \quad (23)$$

Table 5. The $n_{f\,ave}$, $n_{c\,ave}$, r_{B2O3}, and f_{B2O3} of the B_2O_3 of $xBaF_2$–(50 – x)CaF_2 –50B_2O_3 (x = 5 to 35 mol%) glass system

BaF_2 content (mol%)	$n_{f\,ave}$	$n_{c\,ave}$	r_{B2O3} (nm)	f_{B2O3} (N m^{-1})
5	3.330	1.330	0.1406	591.87
10	3.316	1.316	0.1405	496.04
15	3.340	1.340	0.1407	563.36
20	3.335	1.335	0.1407	576.46
25	3.145	1.145	0.1386	496.76
30	3.363	1.363	0.1410	544.52
35	3.344	1.344	0.1408	563.56

Table 5 represents the calculated values of the average coordination number ($n_{f\,ave}$), average cross-link density per cation (nc ave), average bond length (r_{B2O3}), and first-order stretching force constant (f_{B2O3}) of the B-O bonds in the glass samples. According to the bond compression model, the average cross-link density per unit formula, $\bar{n}_c$, was expressed by equation (24) [45]. In this equation, n_c represents the cross-link density per cation (number of bridging bonds per cation minus two), and N_c is the total number of cations in the component. The ideal Poisson's ratio for the poly-component oxide glasses, as determined by the bond compression model, can be calculated using equation (25) [28].

$$\text{Average cross-link density, } \bar{n}_c = \frac{\sum_i x_i (n_c)_i (N_c)_i}{\sum_i x_i (N_c)_i} \tag{24}$$

$$\sigma_{cal} = 0.28(\bar{n}_c)^{-0.25} \tag{25}$$

The bulk compression model suggests an isotropic deformation that alters network bond lengths and sizes without changing in the interatomic bond angles. According to this model, the ring deformation mechanism may occur if the K_{bc}/K_e ratio exceeds 1, indicating a relatively open (or large-ringed) three-dimensional network, with an increase in ring size as the K_{bc}/K_e ratio rises [38]. This network is described as less stable and easily compressed. Meanwhile, ratios approaching 1 indicate a more stable glass structure, where the connection between its structural units strengthens. Conversely, a high K_{bc}/K_e ratio is indicative of a layered and chained network. The non-existence of bonds in specific directions in both types of structure resulted in the bending of the bonds once isotropic force is applied. Consequently, network bond-bending would dominate when the glass sample is subjected to bulk compression.

The Ring Deformation Model

This model relates the ring size of the vitreous network and the K_{bc}/K_e ratio which was proposed by [32]. Based on the model, the increment of ring size (l) in the amorphous network could be observed from the K_{bc}/K_e ratio. Accordingly, a loaded-beam assembly's deformation approach strongly depends on beam lengths. The central depression of a uniformly loaded beam clamped at both ends with a length of l, is proportional to l^4.

Bridge *et al*. (1983) also suggested that the bulk modulus of ring atoms applied with a uniform pressure would predominantly depend on the ring diameter. Any changes in the atomic ring diameter (the number of cation-anion bonds in one ring multiplied by bond length and divided by π) and average first-order stretching force constant would alter the bulk modulus of the glass following the semi-empirical relationship. Consequently, the average ring size diameter of the network could be calculated with equation (26) [28]:

$$l = \left[0.0106 \frac{\bar{F}}{K_e}\right]^{0.26} \quad (26)$$

Where K_e is the experimental bulk modulus and $\bar{F}$ is the glass's average bond stretching force constant from equation (27), employed in multi-component glasses [28]. The x_i, n_f, and f_i in the equation are defined previously.

$$\bar{F} = \frac{\sum_i x_i n_f f_i}{\sum_i x_i n_f} \quad (27)$$

The values of the calculated bulk modulus (K_{bc}), the calculated ratio of K_{bc}/K_e, average cross-link density ($\bar{n}_c$), ideal Poisson's ratio based on the bulk compression model (σ_{cal}), and average stretching force constant ($\bar{F}$) of the glass samples prepared in the present study are listed in Table 6. The K_{bc} decreased as the BaF_2 content increased. Nevertheless, decreased K_{bc} with a minimum of 10 mol% and a large drop at 25 mol% of BaF_2 demonstrated an almost similar pattern with the experimental bulk modulus, K_e (Figure 7). Moreover, based on Figure 8, the *l* fluctuated with a maximum at 10 mol% and 25 mol%, and the K_{bc}/K_e variations exhibited similar values between 1.89–2.24.

Table 6. The calculated bulk modulus (K_{bc}) values based on the bulk compression model, K_{bc}/K_e ratio, ideal Poisson's ratio (σ_{cal}), average ring size (*l*), average bond stretching force constant $\bar{F}$, and average crosslink of the $x BaF_2$–$(50 - x)CaF_2$–$50B_2O_3$ (x = 5 to 35 mol%) glass system

x (mol%)	K_{bc} (GPa)	K_{bc}/K_e	σ_{cal}	*l* (nm)	$\bar{F}$ (N m^{-1})	$\bar{n}_c$
5	129.00	1.89	0.26	0.457	315.65	1.44
10	118.75	2.22	0.25	0.472	280.71	1.46
15	120.91	1.96	0.25	0.459	292.27	1.50
20	119.15	1.91	0.25	0.457	288.57	1.52
25	114.26	2.24	0.26	0.466	235.46	1.45
30	111.65	2.00	0.25	0.460	250.59	1.58
35	110.43	1.93	0.25	0.457	264.58	1.60

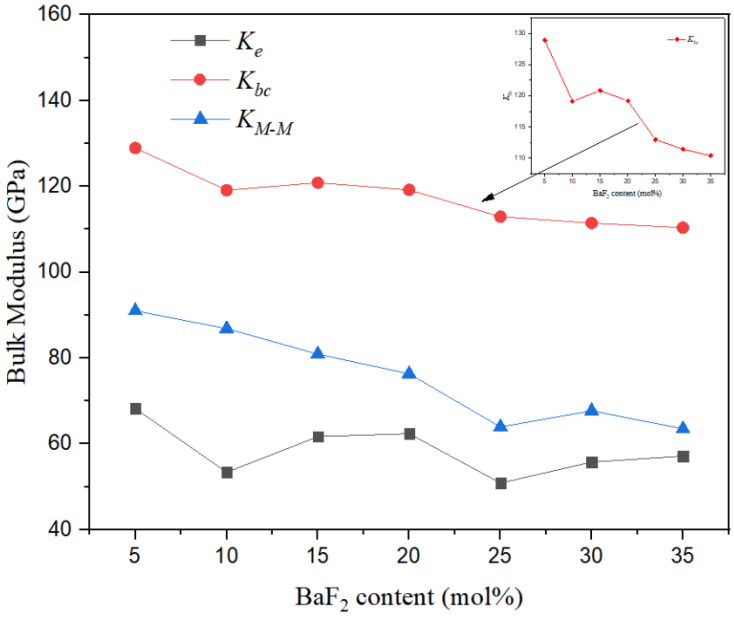

Figure 7. Comparison between the K_e, K_{bc}, and $K_{M\text{-}M}$ of the xBaF$_2$–(50 – x)CaF$_2$ –50B$_2$O$_3$ (x = 5 to 35 mol%) glass system

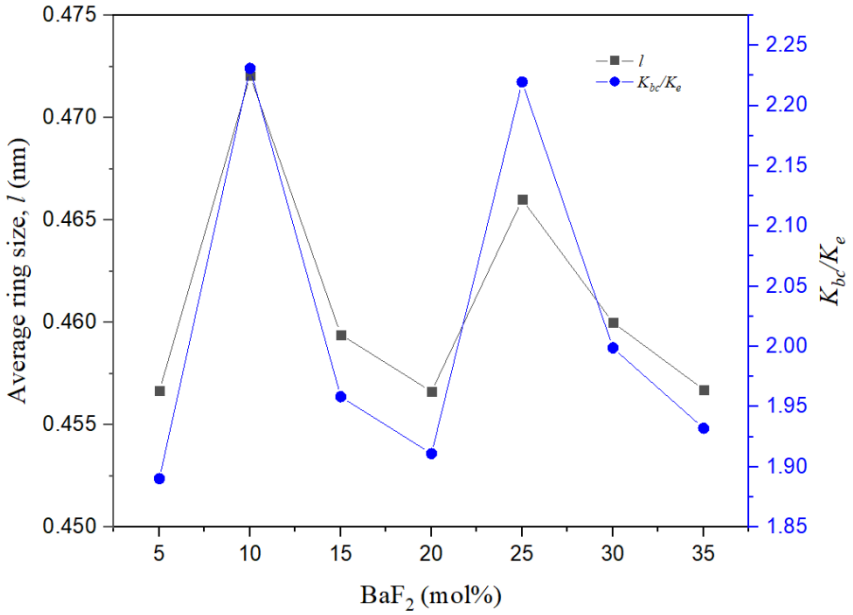

Figure 8. The l and K_{bc}/K_e ratio of the xBaF$_2$–(50 – x)CaF$_2$–50B$_2$O$_3$ (x = 5 to 35 mol%) glass system

Discussion

Density and elastic properties are crucial parameters for exploring the structural properties of glass networks, including compactness, rigidity, geometrical configuration, coordination number, cross-link density, and dimensions of interstitial spaces in the glass [46]. In this study, the glass system exhibited increased ρ (see Figure 1) due to the replacement of the heavier molecular mass of BaF_2 (175.32 g mol^{-1}) with the lighter molecular mass of CaF_2 (78.07 g mol^{-1}). The increased V_m denoted the development of an open structure with more BaF_2, which loosened the network structure, making it less tightly packed [47]. The V_m of the glass samples investigated in this study increased with elevated density, which might be associated with the larger ionic radius of barium (2.68 Å) compared to calcium and boron. Additionally, the longer bond length of BaF_2 (2.32 Å) compared to B_2O_3 (1.48 Å) and CaF_2 (2.10 Å) led to the formation of excess free volume that increased the V_m of the samples [48], [49].

Previous investigations have reported that density strongly influenced elastic velocities, such as v_L and v_S. These velocities are inversely proportional to density and are influenced by the *L* and *S* moduli, which can be calculated using the formula $v_L = \sqrt{L/\rho}$ and $v_S = \sqrt{S/\rho}$. In the present study, it was observed that adding BaF_2 to the glass system decreased v_L and v_S, aligning with these formulas. However, the v_L exhibited nonlinearity, with two minimums at 10 and 25 mol%. Moreover, the v_S decreased between 5–30 mol% with a sharp drop at 20 mol%. Variations in the v_L and v_S values could be understood by examining the behaviours of the independent elastic moduli, *L* and *S*. Based on Figure 3, *S* decreased at $x < 30$ mol%, indicating that the incorporation of BaF_2 might have weakened the glass network, making the glass system less compact and rigid [18]. Furthermore, adding the larger Ba^{2+} ions caused the glass to expand and formed empty spaces.

The *Y* values demonstrated similar behaviours to *S*. The decrease in *Y* (Figure 4) corresponded to a decrease in the stiffness of the glass system. However, beyond 30 mol%, the *Y* and *S* exhibited an abrupt increase, indicating stiffness improvement. This behaviour can be explained by structural reorganisation once Ba^{2+} becomes the dominant modifier. At lower concentrations, Ba^{2+} addition promotes network depolymerisation and non-bridging sites, reducing stiffness. However, above 30 mol% BaF_2, FTIR studies on related systems show that more BO_4 units form [16], raising the N_4 fraction and restoring connectivity. In addition, Ba–F–B bridges likely become more prevalent at higher BaF_2, strengthening the network. These changes explain the observed stiffness improvement in *Y* and *S* at 35 mol% BaF_2.

The bulk modulus, K_e, measures the resistance of a material to uniform compression. As portrayed by equation 6, K_e depends on both the elastic moduli of *L* and *S* [3], [50]. Consequently, the nonlinearity in K_e (Figure 4) with two minimums at x = 10 and 25 mol% might predominantly be due to *L,* which also demonstrated nonlinearity with minima at the same compositions. At 10 mol%, K_e, *L*, and σ showed an anomaly where their values decreased. This can be explained by the formation of non-bridging fluorine (NBF) sites. In the Ca-rich region, additional fluorine introduced by BaF_2 cannot fully integrate as bridging units and instead forms terminal B–F bonds. These NBFs terminate borate chains, reducing compressive stiffness and resulting in minima in K_e and *L*. At 25 mol% BaF_2, FTIR data revealed a drastic reduction in BO_4 units and an increase in BO_3 units, indicating extensive formation of non-bridging oxygens (NBOs). The presence of these NBOs significantly depolymerised the network, again leading to minima in K_e and *L*. The anomaly in σ at 25% is consistent with Ca^{2+} which NBO ionic interactions that compact the structure even though covalent rigidity is reduced.

The apparent inconsistency in attributing anomalies to NBO or NBF can be resolved by considering their relative roles at different compositions. At lower BaF_2 concentrations (≤15 mol%), NBF formation is more prominent, as fluorine produces terminal B–F bonds that depolymerise the network. At equimolar composition (25 mol% BaF_2), the collapse of BO_4 connectivity results in a surge of NBO formation. Both species weaken the structure, but their relative dominance shifts with composition: NBF governs the low-BaF_2 anomaly, while NBO dominates at the equimolar point. This unified interpretation emphasises that the anomalies arise from the overall increase in non-bridging defects, with the type of non-bridging site depending on composition.

At 25 mol%, K_e, *L*, and σ, also recorded a minimum. Intriguingly, ρ and V_m exhibited an off-trend behaviour where ρ increased and V_m decreased abruptly. At this composition, the concentrations of BaF_2 and CaF_2 were equal. A decline in σ might not be expected due to field strength since the mol% of both modifiers were the same. The unusual increase in density and drop in V_m despite network depolymerisation can be explained by Ca^{2+} ions occupying interstitial positions within Ba^{2+}-induced free volume. These smaller Ca^{2+} ions can coordinate with non-bridging oxygens, providing ionic cross-links that contract the structure, increase density, and reduce Poisson's ratio. FTIR spectra at 25% BaF_2 showed a sharp drop in N_4, confirming a lack of BO_4 units, yet density was highest, which implies extra-framework ionic linking. While direct spectroscopic proof of interstitial Ca^{2+} is not available in this study, the combined evidence of densification, σ anomaly, and literature reports of mixed-cation clustering at equimolar ratios strongly support this explanation.

The behaviour of K_e, σ, and V_m might not exhibit a clear correlation since the decrease in K_e should lead to increased V_m and σ of the glass. The rare behaviour was believed to be due to MAEE at 25 mol%, where the BaF_2 and CaF_2 content was at 1:1. In other studies on glass MAEE, composition with a similar ratio also exhibited anomalies [51]. For example, in a study on the composition of $(40 - x)SrO{-}xBaO{-}45SiO_2{-}10B_2O_3{-}5ZrO_2$ glass, deviation from linearity at 20 mol% was assumed to be due to the presence of two alkaline modifiers, leading to several phase separation and disturbing cross-linkages in the glass matrix.

The θ_D is a vital parameter in studying elastic properties corresponding to the temperature at which nearly all lattice vibrations in a solid material are excited. An elevated θ_D indicates the glass network's high interatomic bond strength and rigidity [30]. Based on equation 7, θ_D depends on the number of atoms in chemical composition (P), V_m, and v_m. The strong influence of elasticity on θ_D denoted the significant effect of v_m on θ_D due to the generally similar behaviours between θ_D and v_m. The reduced θ_D and v_m values up to 30 mol%, accompanied by a decrease in the lattice vibrations, indicated a decline in the average rigidity and stiffness in the region. The observations supported the data obtained from the elastic moduli S and Y, as well as V_m.

The value of σ is defined as the ratio of transverse (lateral) to longitudinal (axial) strain produced when a tensile force is applied. Typically, the parameter depends on the dimensionality of the structure and is inversely affected by changes in n_c of the glass network. According to Bridge *et al*., the cross-link density of two, one, and zero are associated with σ values of 0.15, 0.3, and 0.4, respectively. In the present study, σ values ranged from 0.24 to 0.30, indicating an average cross-link per cation between one and two. This range suggests a medium resistance to lateral expansion, typical of a covalently bonded network. The results coincided with a previous study on borate glass [3].

The elastic moduli of S and Y exhibited a sharp decrease at 20 mol% of BaF_2 which could also be observed in the θ_D and v_m. Nonetheless, K_e exhibited maxima at a similar BaF_2 content. This observation could depict the interstitial occupation of Ba^{2+} that replaced the Ca^{2+} in the borate structure, resulting in an abrupt weakening in the borate structure. Nevertheless, compression was tougher with the formation of B_4 units. The scenario might indicate that the region involved a complex structural adjustment related to the MAEE that is yet entirely comprehended.

The Makishima-Mackenzie model estimated the elastic moduli by calculating the bond strength from the dissociation energy and bond density using specific bond energy and atomic packing fraction. The results show that the calculated moduli for $L_{M\text{-}M}$, $K_{M\text{-}M}$, $Y_{M\text{-}M}$, and $S_{M\text{-}M}$ were higher than the experimentally obtained values. This discrepancy can be attributed to the glass bonds' higher packing density and dissociation energy values. Nevertheless, the theoretical elastic moduli decreased slightly, sharply dropping at 25 mol%. The decrease in calculated values supports the decrease in stiffness observed in the experimental elastic moduli. Additionally, the data suggest that the strength of atomic bonds in the glass structure becomes weaker even with enhanced density.

The sudden drop in calculated elastic moduli at 25 mol% of BaF_2 may be influenced by the value of N_4, which exhibited a significant and drastic drop at the same composition, indicating signs of MAEE. Moreover, the sudden decrease in elastic moduli (M-M model) at 25 mol% coincided with the minimum recorded by elastic moduli L and K_e. As reported in a previous FTIR study, this behaviour can be attributed to forming a large NBO. The observation may also be due to the dissociation energy of the borate with coordination number three, which is much lower than that of the borate with coordination number four. At 25 mol%, the N_4 value is much lower than in other compositions, indicating a greater proportion of borate units with coordination number three. However, L and K_e also have a minimum at 10 mol%, but the minimum is not demonstrated in the theoretical elastic moduli based on the Makishima-Mackenzie model. The anomaly at 10 mol% may not be caused by dissociation energy due to changes in bonds but by other factors that cannot be ascertained.

In the bulk compression model, the ideal bulk modulus (K_{bc}) was calculated based on the assumption that each covalent bond within the glass network experiences ideal compression, requiring higher compression than experimental bulk compression. The K_{bc} values decrease with the increased BaF_2 concentration in the current study, with a slight drop occurring at 10 and 25 mol%. According to the bulk compression and ring deformation models, the average stretching force constant ($\bar{F}$) decreases with increased BaF_2 content, resulting in a change in K_{bc} that also affects a change in the ring diameter, as shown in Figure 8. The changes in the bulk compression model, similar to the variations observed in the experimental bulk modulus, support the change in elastic modulus. The average stretching force, $\bar{F}$, the number of network bonds per unit volume, and the average coordination number also affect the alterations.

According to the ring deformation model, K_{bc}/K_e is greater than one, indicating the presence of ring deformation alongside isotropic elastic compression [50]. Nevertheless, the present work demonstrates K_{bc}/K_e values within 1–3, denoting that the main compression mechanism of the glass system is isotropic ring compression. In the current study, the K_{bc}/K_e ratios are maxima at x = 10 and 25 mol%, coinciding with the anomalies on some elastic moduli. The larger K_{bc}/K_e ratio reveals the reduction in isotropic compression due to bending or ring deformation between structural units. Similarly, the maximum I obtained from both compositions indicates ring size enlargements, possibly due to large open ring

structures forming. The findings also demonstrated that the elevated ring deformation reduces resistance, explaining the large K_{bc}/K_e ratio value from similar concentrations.

Although the discussion above focuses on structural interpretation, the MAEE-induced elastic anomalies also offer valuable opportunities for engineering applications. Compositions outside the anomaly windows (<10 mol% or >30 mol% BaF_2) exhibit stable rigidity, making them suitable for structural optical components. Intermediate compositions (around 25 mol% BaF_2) combine high density with reduced stiffness, which is advantageous for acoustic damping layers or radiation shielding, where energy absorption and impact tolerance are required. The ability to tune acoustic velocities and Poisson's ratio may be harnessed in acousto-optic devices and laser host media, while dielectric measurements on the same glass system suggest potential in electronic substrates that require both compliance and controlled permittivity. In this way, the non-linear elastic behaviour can be viewed not as a limitation but as a means to tailor glass compositions for specific advanced applications.

Conclusions

This study investigated the elastic properties of $x BaF_2$–$(50 - x)CaF_2$–$50B_2O_3$ (x = 5 to 35 mol%) glasses and revealed pronounced non-linear trends consistent with the mixed alkaline earth effect (MAEE). Measurements of density, ultrasonic velocities, and elastic moduli (*Y, S, L,* K_e, and σ) showed anomalies at 10 and 25 mol% BaF_2. These deviations were explained by structural rearrangements within the glass network: at lower BaF_2 concentrations, excess fluorine introduced non-bridging fluorine (NBF) sites that disrupted connectivity, while at the equimolar Ca/Ba ratio, extensive non-bridging oxygen (NBO) formation dominated, depolymerising the network. The unusual densification at 25 mol% BaF_2, despite reduced BO_4 connectivity, was attributed to Ca^{2+} ions occupying interstitial positions and coordinating with NBOs, thereby providing ionic cross-links. Collectively, these mechanisms demonstrate that both NBO and NBF formation, as well as modifier rearrangements, contribute to the MAEE.

Theoretical modelling supported these observations. The bond compression model showed good agreement with the experimental data, with minima in K_e and K_{bc} at 10 and 25 mol% reflecting changes in stretching force, bond density, and coordination number. The ring deformation model further indicated that isotropic ring compression was the dominant mechanism, with maxima in I at 10 and 25 mol% corresponding to ring size enlargements caused by BaF_2 substitution and increased NBO concentration, respectively. In contrast, the Makishima–Mackenzie model showed no anomaly at 10 mol%, confirming that the behaviour there was not driven by changes in bond dissociation energy but rather by compressive-type deformation, as predicted by the bulk compression model.

Beyond structural interpretation, the results carry important implications for applications. Compositions outside the anomaly windows (<10 and >30 mol% BaF_2) exhibited stable rigidity and are suitable for optical components requiring predictable stiffness. In contrast, intermediate compositions (around 25 mol% BaF_2) offered high density but reduced stiffness, a combination useful for acoustic damping layers, protective or radiation-shielding glasses, and substrates where impact absorption is advantageous. The tunability of acoustic velocities and Poisson's ratio further suggests potential for acousto-optic devices, laser host media, and dielectric substrates, where mechanical compliance can be matched to functional requirements.

Overall, the study demonstrates that elastic anomalies arising from the MAEE are not limitations but opportunities: by adjusting modifier ratios, glasses with tailored mechanical and functional properties can be engineered for advanced technological applications.

Conflicts of Interest

The authors declare that there is no conflict of interest regarding the publication of this paper.

Acknowledgment

This study was supported by Ministry of Higher Education (MOHE), Malaysia through project grant of Fundamental Research Grant Scheme (FRGS) FRGS/1/2019/STG07/UITM/03/6.
.

References

[1] Maniua, D., Iliescu, T., Ardelean, I., Cinta-Pinzaru, S., Tarcea, N., & Kiefer, W. (2003). Raman study on B_2O_3–CaO glasses. *Journal of Molecular Structure*, 485–488. https://doi.org/10.1016/S0022-2860(03)00129-7.

[2] Kaur, G., Pandey, O. P., & Singh, K. (2012). Effect of modifiers field strength on optical, structural and mechanical properties of lanthanum borosilicate glasses. *Journal of Non-Crystalline Solids*, *358*(18–19), 2589–2596. https://doi.org/10.1016/j.jnoncrysol.2012.06.006.

[3] Sabri, N. S., Yahya, A. K., Abd-Shukor, R., & Talari, M. K. (2016). Anomalous elastic behaviour of xSrO–10PbO–(90–x)B_2O_3 glass system. *Journal of Non-Crystalline Solids*, *444*, 55–63. https://doi.org/10.1016/j.jnoncrysol.2016.04.038.

[4] Sabri, N. S., Yahya, A. K., & Talari, M. K. (2017). Anomalous optical properties of xSrO–10PbO–(90–x)B_2O_3 glass system. *Transactions of the Indian Institute of Metals*, *70*(3), 557–565. https://doi.org/10.1007/s12666-017-1043-8.

[5] Abousehly, A., Issa, S. A. M., El-Oyoun, M. A., & Afify, N. (2015). Electrical and mechanical properties of Li_2O–BaO–B_2O_3 glass system. *Journal of Non-Crystalline Solids*, *429*, 148–152. https://doi.org/10.1016/j.jnoncrysol.2015.09.003.

[6] Yiannopoulos, Y. D., Chryssikos, G. D., & Kamitsos, E. I. (2001). Structure and properties of alkaline earth borate glasses. *Physics and Chemistry of Glasses*.

[7] Narayanan, M. K., & Shashikala, H. D. (2015). Thermal and optical properties of BaO–CaF_2–P_2O_5 glasses. *Journal of Non-Crystalline Solids*, *422*, 6–11. https://doi.org/10.1016/j.jnoncrysol.2015.04.038.

[8] Krishna Murthy, M., Murthy, K. S. N., & Veeraiah, N. (2000). Dielectric properties of NaF–B_2O_3 glasses doped with certain transition metal ions. *Bulletin of Materials Science*, *23*(4), 285–293. https://doi.org/10.1007/BF02720084.

[9] El-Egili, K., Doweidar, H., Ramadan, R., & Altawaf, A. (2016). Role of F^- ions in the structure and properties of BaF_2–B_2O_3 glasses. *Journal of Non-Crystalline Solids*, *449*, 83–93. https://doi.org/10.1016/j.jnoncrysol.2016.07.014.

[10] Doweidar, H., El-Damrawi, G., & Abdelghany, M. (2012). Structure and properties of CaF_2–B_2O_3 glasses. *Journal of Materials Science*, *47*(9), 4028–4035. https://doi.org/10.1007/s10853-012-6256-y

[11] Kamitsos, E. I., & Karakassides, M. A. (1988). A spectroscopic study of fluoride containing sodium borate glasses. *Solid State Ionics*, *28–30*, 783–787.

[12] Bih, L., Abbas, L., Mohdachi, S., & Nadiri, A. (2008). Thermal and electrical properties of mixed alkali in Li_2O–Na_2O–WO_3–P_2O_5 glasses. *Journal of Molecular Structure*, *891*(1–3), 173–177. https://doi.org/10.1016/j.molstruc.2008.03.019.

[13] Japari, S. J., Yahya, A. K., & Hisam, R. (2020). Effects of mixed-alkali oxides on AC conductivity and dielectric properties of xNa_2O–(20–x)K_2O–30V_2O_5–50TeO_2 glasses. *Results in Physics*, *16*, 102905. https://doi.org/10.1016/j.rinp.2019.102905.

[14] Calahoo, C., & Zwanziger, J. W. (2017). The mixed modifier effect in ionic conductivity and mechanical properties for xMgO–(50–x)CaO–50SiO_2 glasses. *Journal of Non-Crystalline Solids*, *460*, 6–18. https://doi.org/10.1016/j.jnoncrysol.2017.01.017

[15] Walia, T., & Singh, K. (2021). Mixed alkaline earth modifiers effect on thermal, optical and structural properties of SrO–BaO–SiO_2–B_2O_3–ZrO_2 glass sealants. *Journal of Non-Crystalline Solids*, *564*, 120812. https://doi.org/10.1016/j.jnoncrysol.2021.120812.

[16] Sahapini, N. F. M., Hisam, R., & Yahya, A. K. (2022). Structural and optical properties of mixed alkaline earth fluoroborate xBaF_2–(50–x)CaF_2–50B_2O_3 glass system. *Applied Physics A*, *128*(3), 223. https://doi.org/10.1007/s00339-022-05360-z.

[17] Inaba, S., Fujino, S., & Morinaga, K. (1999). Young's modulus and compositional parameters of oxide glasses. *Journal of the American Ceramic Society*, *82*(12), 3501–3507. https://doi.org/10.1111/j.1151-2916.1999.tb02272.x.

[18] Mohamed, N. B., Yahya, A. K., Deni, M. S. M., Mohamed, S. N., Halimah, M. K., & Sidek, H. A. A. (2010). Effects of concurrent TeO_2 reduction and ZnO addition on elastic and structural properties of (90–x)TeO_2–10Nb_2O_5–xZnO glass. *Journal of Non-Crystalline Solids*, *356*(33–34), 1626–1630. https://doi.org/10.1016/j.jnoncrysol.2010.06.031.

[19] Shaaban, K. S., Sayed, M. A., Saddeek, Y. B., & Yahia, I. S. (2019). Structural analyses of halide alkali lead borate glasses. *Silicon*, *11*(5), 2413–2419. https://doi.org/10.1007/s12633-016-9465-1

[20] El-Moneim, A. A. (2018). Theoretical analysis for ultrasonic properties of vanadate glasses over a wide range of composition. *Journal of Non-Crystalline Solids*, *498*, 134–144. https://doi.org/10.1016/j.jnoncrysol.2018.06.010.

[21] El-Hofy, M., & Hager, I. Z. (2003). Ionic conductivity in lithium haloborate glasses. *Physica Status Solidi A: Applied Research*, *199*(3), 448–456. https://doi.org/10.1002/pssa.200306670.

[22] Patil, S. D., Jali, V. M., & Anavekar, R. V. (2009). Elastic properties of Na_2O–ZnO–ZnF_2–B_2O_3 oxyfluoride glasses. *Bulletin of Materials Science*, *32*(6), 597–601.

[23] Hager, I. Z. (2002). Elastic moduli of boron oxyfluoride glasses: Experimental determinations and application of Makishima and Mackenzie's theory. *Journal of Materials Science*, *37*, 1309–1313.

[24] El-Mallawany, R., Afifi, H. A., El-Gazery, M., & Ali, A. A. (2018). Effect of Bi_2O_3 addition on the ultrasonic properties of pentaternary borate glasses. *Measurement*, *116*, 314–317. https://doi.org/10.1016/j.measurement.2017.11.028.

[25] Ismail, M., Supardan, S. N., Yahya, A. K., Yusof, M. I. M., & Halimah, M. K. (2016). Anomalous elastic and optical behaviours of mixed electronic-ionic of xAg_2O−(35−x)[0.5MoO_3−0.5V_2O_5]−65TeO_2 conductor glasses. *Chalcogenide Letters*, *13*(11), 989–1005.

[26] Umair, M. M., & Yahya, A. K. (2015). Effect of Nb_2O_5 network stabilizer on elastic and optical properties of

xNb_2O_5–(20–x)BaO–80TeO_2 tellurite glass system. *Journal of the American Ceramic Society*, *12*(6), 287–300. https://doi.org/10.1111/j.1551-2916.2006.01399.x.

[27] Hisam, R., & Yahya, A. K. (2016). Anomalous behaviours of elastic moduli, DC conductivity and optical properties in mixed transition-metal-ion (20–x)MnO_2–xFe_2O_3–8TeO_2 tellurite glass system. *Chalcogenide Letters*, *13*(4), 145–160.

[28] Samsudin, N. M., Hisam, R., & Yahya, A. K. (2021). Structural, DC conductivity and elastic properties of (80–x)B_2O_3–xTeO_2–10Li_2O–10Al_2O_3 mixed glass former. *Ionics*, *27*(2), 619–634. https://doi.org/10.1007/s11581-020-03859-0.

[29] Samdani, G., Ramadevudu, M., Chary, M. N., & Shareefuddin, M. (2017). Physical and spectroscopic studies of Cr^{3+} doped mixed alkaline earth oxide borate glasses. *Materials Chemistry and Physics*, *186*. https://doi.org/10.1016/j.matchemphys.2016.11.009.

[30] Azianty, S., & Yahya, A. K. (2013). Enhancement of elastic properties by WO_3 partial replacement of TeO_2 in ternary (80–x)TeO_2–20PbO–xWO_3 glass system. *Journal of Non-Crystalline Solids*, *378*, 234–240. https://doi.org/10.1016/j.jnoncrysol.2013.07.016.

[31] Makishima, A., & Mackenzie, J. D. (1975). Calculation of bulk modulus, shear modulus and Poisson's ratio of glass. *Journal of Non-Crystalline Solids*, *17*(2), 147–157. https://doi.org/10.1016/0022-3093(75)90047-2.

[32] Bridge, B., Patel, N. D., & Waters, D. N. (1983). On the elastic constants and structure of the pure inorganic oxide glasses. *Physica Status Solidi (a)*, *77*, 655–668.

[33] Halimah, M. K., Daud, W. M., & Sidek, H. A. A. (2010). Elastic properties of TeO_2–B_2O_3–Ag_2O glasses. *Ionics*, *16*(9), 807–813. https://doi.org/10.1007/s11581-010-0465-7.

[34] Matecki, M., & Lucas, J. (1994). Elastic moduli of fluoride glasses: Application of Makishima and Mackenzie's theory. *Materials Research Bulletin*, *29*(5), 473–477.

[35] Shi, Y., Tandia, A., Deng, B., Elliott, S. R., & Bauchy, M. (2020). Revisiting the Makishima–Mackenzie model for predicting the Young's modulus of oxide glasses. *Acta Materialia*, *195*, 252–262. https://doi.org/10.1016/j.actamat.2020.05.047.

[36] Hager, I. Z. (2002). Elastic moduli of boron oxyfluoride glasses: Experimental determinations and application of Makishima and Mackenzie's theory. *Journal of Materials Science*, *37*(7), 1309–1313. https://doi.org/10.1023/A:1014552008442.

[37] Batsanov, S. S., & Batsanov, A. S. (2013). *Introduction to structural chemistry*. Springer Netherlands. https://doi.org/10.1007/978-94-007-4771-5.

[38] Abd El-Moneim, A. (2018). BaF_2-contained tellurite glasses: Quantitative analysis and prediction of elastic properties and ultrasonic attenuation–Part I. *Journal of Fluorine Chemistry*, *210*, 156–165. https://doi.org/10.1016/j.jfluchem.2018.03.005

[39] El-Moneim, A. A. (2019). Correlating bulk modulus and Poisson's ratio of alkali fluoride and oxyfluoride glasses with compositional parameters. *Journal of Fluorine Chemistry*, *221*, 48–55.

[40] El-Mallawany, R., Hager, I. Z., & Poulain, M. (2002). Thermal properties of new molybdenum oxyfluoride glasses. *Journal of Materials Science*, *37*, 3291–3297.

[41] Kamitsos, E. I., & Chryssikos, G. D. (1991). Borate glass structure by Raman and infrared spectroscopies. *Journal of Molecular Structure*, *247*, 1–16.

[42] Wright, A. C., Vedishcheva, N. M., & Shakhmatkin, B. A. (1995). Vitreous borate networks containing superstructural units: A challenge to the random network theory? *Journal of Non-Crystalline Solids*, *192–193*, 92–97.

[43] Saddeek, Y. B. (2004). Ultrasonic study and physical properties of some borate glasses. *Materials Chemistry and Physics*, *83*(2–3), 222–228. https://doi.org/10.1016/j.matchemphys.2003.09.051.

[44] Saddeek, Y. B. (2004). Structural analysis of alkali borate glasses. *Physica B: Condensed Matter*, *344*(1–4), 163–175. https://doi.org/10.1016/j.physb.2003.09.254.

[45] Umair, M. M., & Yahya, A. K. (2013). Elastic and structural changes of xNa_2O–(35–x)V_2O_5–65TeO_2 glass system with increasing sodium. *Materials Chemistry and Physics*, *142*(2–3), 549–555. https://doi.org/10.1016/j.matchemphys.2013.07.051.

[46] Nishara Begum, A., & Rajendran, V. (2006). Structure and elastic properties of TeO_2–BaF_2 glasses. *Journal of Physics and Chemistry of Solids*, *67*(8), 1697–1702. https://doi.org/10.1016/j.jpcs.2006.03.007.

[47] Edukondalu, A., Ramadevudu, G., Chary, M. N., & Shareefuddin, M. (2012). Mixed alkali effect in physical and optical properties of Li_2O–Na_2O–WO_3–B_2O_3 glasses. *Journal of Non-Crystalline Solids*, *358*(18–19), 2581–2588. https://doi.org/10.1016/j.jnoncrysol.2012.06.004.

[48] Garza-Garcia, M., Lopez-Cuevas, J., Gutierrez-Chavarria, C. A., Rendon-Angeles, J. C., & Valle-Fuentes, J. F. (2007). Study of a mixed alkaline-earth effect on some properties of glasses of the CaO–MgO–Al_2O_3–SiO_2 system. *Boletín de la Sociedad Española de Cerámica y Vidrio*, *46*(3), 153–162.

[49] Seijo, L., Barandiarán, Z., & Huzinaga, S. (1991). *Ab initio* model potential study of the equilibrium geometry of alkaline earth dihalides: MX_2 (M = Mg, Ca, Sr, Ba; X = F, Cl, Br, I). *Journal of Chemical Physics*, *94*(5), 3762–3773. https://doi.org/10.1063/1.459748.

[50] Mohamed, S. N., & Yahya, A. K. (2018). Effects of V_2O_5 on elastic, structural, and optical properties of mixed ionic–electronic 20Na_2O–20CaO–(60–x)B_2O_3–xV_2O_5 glasses. *Ionics*, *24*(9), 2647–2664. https://doi.org/10.1007/s11581-017-2396-z.

[51] Guo, H. W., Wang, X. F., Gong, Y. X., & Gao, D. N. (2010). Mixed alkali effect in xK_2O–(30–x)Na_2O–30P_2O_5–40ZnO glasses. *Journal of Non-Crystalline Solids,* *356*(41–42), 2109–2113. https://doi.org/10.1016/j.jnoncrysol.2010.07.060.